Published online 3 November 2011 *Nucleic Acids Research, 2012, Vol. 40, No. 4* ***1807–1817***
doi:10.1093/nar/gkr835

Conformational dynamics of the tetracycline-binding aptamer

Ute Förster[1], Julia E. Weigand[2], Peter Trojanowski[1], Beatrix Suess[2,*] and Josef Wachtveitl[1,*]

[1]Institut für Physikalische und Theoretische Chemie, Goethe-Universität Frankfurt, Max-von-Laue-Straße 7 and [2]Institut für Molekulare Biowissenschaften, Goethe-Universität Frankfurt, Max-von-Laue-Straße 9, D-60438 Frankfurt am Main, Germany

Received February 23, 2011; Revised September 16, 2011; Accepted September 20, 2011

ABSTRACT

The conformational dynamics induced by ligand binding to the tetracycline-binding aptamer is monitored via stopped-flow fluorescence spectroscopy and time-correlated single photon counting experiments. The fluorescence of the ligand is sensitive to changes within the tertiary structure of the aptamer during and after the binding process. In addition to the wild-type aptamer, the mutants A9G, A13U and A50U are examined, where bases important for regulation are changed to inhibit the aptamer's function. Our results suggest a very fast two-step-mechanism for the binding of the ligand to the aptamer that can be interpreted as a binding step followed by a reorganization of the aptamer to accommodate the ligand. Binding to the two direct contact points A13 and A50 was found to occur in the first binding step. The exchange of the structurally important base A9 for guanine induces an enormous deceleration of the overall binding process, which is mainly rooted in an enhancement of the back reaction of the first binding step by several orders of magnitude. This indicates a significant loss of tertiary structure of the aptamer in the absence of the base A9, and underlines the importance of pre-organization on the overall binding process of the tetracycline-binding aptamer.

INTRODUCTION

During the last years, the folding dynamics of aptamers and riboswitches as well as the formation of RNA–ligand complexes have been examined in various contexts. A variety of time-resolved spectroscopic techniques (1) such as NMR (2–5), also in combination with the ultrafast release of caged ligands (6) and fluorescence stopped-flow have been applied. The latter has been based both on fluorescent ligands (7–9) and the fluorescent adenine derivate 2-aminopurine (7,10–12), the lifetime of which can also be used to gain information on the RNA conformation (13). The monitoring of fluorescent ligands has mostly led to the observation of one-step binding processes (7–9,11), however, when monitoring different parts of the same aptamer, varying conformational dynamics were found, leading to a significantly more complex overall picture (11,13). A central, but unresolved issue is the notion of pre-organization of the RNA before ligand recognition to accommodate binding. These references provide discussion of conformational capture (14) and induced fit mechanisms for a variety of systems (15).

The tetracycline-binding aptamer (Figure 1) identified by *in vitro* selection [SELEX; (16)], is an interesting genetic device for application in synthetic biology. It has been used for conditional control of translation initiation (17–19) and pre-mRNA splicing in yeast (20). In both cases, the aptamer–ligand complex interferes with protein functions either by steric hindrance or masking of binding sites.

The aptamer resembles a complex h-shaped structure with the ligand-binding site in the centre of the three-way junction [Figure 1C; (21)]. The core of the aptamer is formed by an irregular triple helix resulting from both joining regions J1-2 and J2-3 and nucleotides of loop L3. A base triplet between A9, A44 and A55 forms the basis of the triple helix (Figure 1D).

The ligand tetracycline (Figure 1B) binds within this interface as a magnesium ion chelate with a sub-nanomolar dissociation constant of 770 pM (22). Thermodynamic analysis and the crystal structure of the aptamer–ligand complex give insight into a variety of interactions between the aptamer and its ligand (21,22). A main contact occurs at the adenine nucleotide A13 from the joining region J1-2 which forms two hydrogen bonds

*To whom correspondence should be addressed. Tel: +49 (0)69 798 29351; Fax: +49 (0)69 798 29709; Email: wveitl@theochem.uni-frankfurt.de
Correspondence may also be addressed to Beatrix Suess. Tel: +49 (0)69 798 29785; Fax: +49 (0)69 798 29323; Email: suess@bio.uni-frankfurt.de

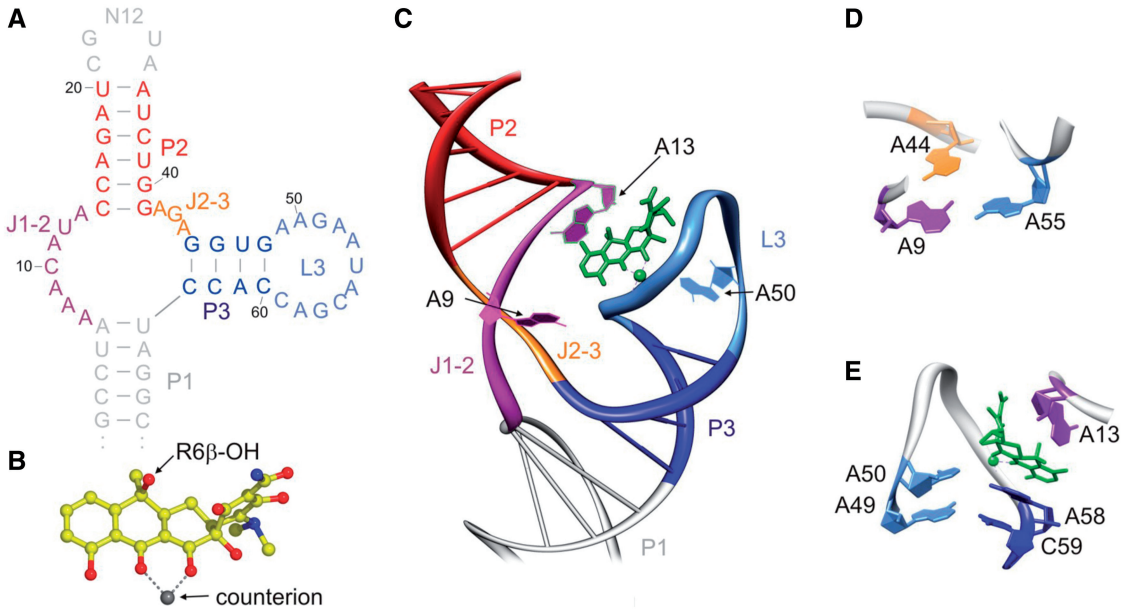

Figure 1. The tetracycline-binding aptamer. (**A**) Secondary structure and (**C**) crystal structure (21) of the tetracycline-binding aptamer. Stem regions P1-P3, the joining regions J1-2 and J2-3 and the loop L3 are colored and marked. Tetracycline is shown as green stick model, magnesium as green ball. (**B**) Ball and stick representation of tetracycline. (**D**) The base triplet between A9, A44 and A55, which forms the basis of the triple helix. (**E**) Location of the nucleotides A13 and A50 with respect to tetracycline.

to the 6β-OH group of tetracycline (Figure 1E). The β-hydroxyketone moiety of tetracycline is deeply buried in the RNA with ring CD stacking on A58 of the loop L3. A58 together with A50 indirectly recognize the ligand via hydrogen bonds to a coordinating water molecule of the tetracycline's counterion (Figure 1E) (21). It is, as of now, unclear, to which extent the tertiary structure is already formed in the absence of ligand. However, genetic, biochemical and biophysical data suggest significant pre-organization on the secondary and tertiary structural level (22–24).

This work now focuses on the binding dynamics of the tetracycline aptamer and the structural confinement of tetracycline in the binding pocket. Both properties are monitored via the tetracycline fluorescence that is strongly enhanced upon binding to the aptamer (22). Thus, it provides a sensitive probe to monitor the binding process and conditions by means of fluorescence spectroscopy (25). The fluorescence lifetime of the chromophore is used to report on its general confinement, while the change in tetracycline quantum efficiency is used for a real-time observation of the binding events.

MATERIAL AND METHODS

Preparation of aptamer RNA

Aptamer RNA was transcribed *in vitro* from a linearized pSP64 plasmid (Promega) using T7 polymerase. For precise aptamer 3′-ends, the primary transcripts contained self-cleaving hammerhead ribozymes (Supplementary Figure S1). Run-off transcription was performed as previously described (22). After *in vitro* transcription and ethanol precipitation, the RNA products were separated on an 8% denaturing polyacrylamide gel, detected by ultraviolet shadowing and gel eluted. After a second ethanol precipitation, the RNA was resuspended in H_2O and stored frozen at −20°C.

RNA concentrations were calculated with aptamer specific extinction coefficients using the 'Oligonucleotide MW and Extinction Coefficient Calculator' from Ambion (http://www.ambion.com/techlib/misc/oligo_calculator.html). The tetracycline concentration was determined measuring the optical density at the absorption maximum in water (26).

Yeast tRNA (Invitrogen) was used as non-specific RNA control. For all fluorescence measurements, RNA and tetracycline stock solutions were prepared in water and diluted with a 5-fold concentrated buffer (final buffer conditions: 20 mM potassium phosphate pH 7.5, 100 mM NaCl and 10 mM $MgCl_2$). For the fluorescence lifetime measurements in the TCSPC setup, samples were prepared at equal concentrations of RNA and tetracycline at 20 μM in the above mentioned buffer, stopped-flow measurements were carried out at varying concentrations, which are given at each individual measurement.

Time correlated single photon counting

A detailed description of the combined TCSPC/Upconversion setup has been described in detail previously (27). In short, pulses of a Spectra Physics Tsunami-Spitfire-system (Newport Spectra Physics, Irvine, California) operating at 770 nm at a pulse width of 130 fs and pulse energy of 1 mJ per pulse were frequency doubled. The excitation energy at 385 nm was tuned to 100 nJ.

Fluorescence was separated spatially and with a FGL435-filter from the excitation light and then passed

through a Jobin Yvon Gemini 180 double monochromator (HORIBA Jobin-Yvon, Munich, Germany). Detection was carried out using a cooled single photon counting detector head PMC 100-4 (Becker & Hickl, Berlin, Germany). TCSPC data acquisition was managed by a Becker & Hickl MSA 1000 counting system (Becker & Hickl, Berlin, Germany). It provides a channel width of 1 ns and a maximum number of 1024 channels. A fused silica cuvette with 1 mm optical path length was used and moved in two dimensions perpendicular to the incident beam to avoid excessive photobleaching. A total of 25 measurements have been carried out at different wavelengths between 460 and 580 nm, using 60 000 cycles per transient.

Absorption spectra were taken before and after the measurement to estimate the photobleaching within the sample during the measurement. In all experiments reported here no photobleaching was observed.

Data analysis was carried out using a global fit analysis routine on the basis of a Levenberg-Marquart algorithm assuming a Gaussian-shaped cross correlation of 1.2 ns.

Stopped-flow spectroscopy

Stopped-flow transients were taken in a Jasco SFM-20 Stopped-flow setup (Jasco, Groß-Umstadt, Germany) using a cuvette (FC08) with an approximate volume of 20 µl and a light path of 0.8 mm, which results in a dead time of 1.6 ms. The samples were excited with a UV LED at 375 nm (PUR LED, Hahnheim, Germany). The channel width was set to 20 µs for all measurements. Fluorescence was collected under an angle of 90°. The emission light was separated from the excitation by two filters with a cut-off wavelength of 435 nm (FGL435, ThorLabs, Karlsfeld, Germany) and detected by a Hamamatsu PMT H9656-20 photomultiplier (Hamamatsu Deutschland, Herrsching, Germany). Both light source and detector were placed close to the cuvette to minimize intensity loss due to stray light. A series of measurements were carried out for the wild-type and all three mutants, where for two different aptamer concentrations the tetracycline concentration was varied over a wide range (details are given in each figure). A control experiment with non-specific tRNA is shown in Supplementary Figure S4 to reassure that no unspecific binding occurs. The data were averaged over 20 (for the higher RNA concentration of ~7 µM) or 40 (for the lower RNA concentration of ~2 µM) identical measurements.

Prior to fitting, all transients were corrected for the fluorescence signal of unbound tetracycline by subtracting a constant offset from every transient. The transients were normalized, taking into account an estimate of the system evolution during the instrumental dead time, a correction for LED drift and the total concentration of RNA–tetracycline complexes in the sample (details on the normalization procedure, see Supplementary Figure S2).

Each set of transients was processed using the Dynafit software (28,29) (Biokin Ltd., Watertown, USA) to test different and to derive the appropriate reaction model and reaction constants (details on the fitting procedure, see Supplementary Figures S2, S3 and Supplementary Table S1).

RESULTS

Tetracycline binds to the aptamer in a two-step process

Stopped-flow-measurements allow monitoring dynamic processes in the time range of milliseconds to seconds. We used this technique to monitor the formation of the tetracycline aptamer complex in a time-resolved manner. The steady-state fluorescence of the tetracycline was used as a reporter signal similar as for the previously reported equilibrium binding constant measurements (22).

The binding dynamics of the tetracycline-binding aptamer was recorded at room temperature using two different aptamer concentrations of 1.8 and 6.8 µM. The corresponding tetracycline concentrations were varied between 6–46 µM and 12–101 µM, respectively. Figure 2A shows the measured set of transients. Binding of tetracycline to the aptamer leads to a significant increase in fluorescence. In contrast, no fluorescence increase was observed for tRNAs as a non-specific RNA control (Supplementary Figure S4). The binding dynamics of the wild-type aptamer is extremely fast and increases with rising tetracycline concentrations. In the observed concentration range, complete ligand binding is induced well below 50 ms. This is two to three orders of magnitude faster than it has been observed for the aptamer domains of several riboswitches such as the FMN, TPP or the adenine riboswitch (6,8,9,12) and is in accordance with the remarkably low K_D of the tetracycline-binding aptamer.

The collected data have been fitted using the program Dynafit. A number of different reaction models were assumed and their root-mean-square deviations and the overall reaction constants compared with each other (for details see Supplementary Figure S3 and Supplementary Table S1). A comparative analysis of several one-step, two-step and three-step models showed, that a one-step model cannot describe the data sufficiently, while a three-step model shows no significant improvement over a two-step model. The first step was found to be reversible, while the additional assumption of a reversible second step yields negligible back reaction rates. This leads to the conclusion, that a two-step mechanism with an irreversible second step is the most probable reaction path for the binding of tetracycline to the aptamer. Figure 2B shows selected transients for both aptamer concentrations and their respective fits. The resulting reaction constants are given in Table 1.

The first step induces a significant fluorescence rise, adding up to slightly <50% of the total fluorescence increase indicating a significant conformational restriction of the chromophore. The formation rate is $13.1 \pm 0.1\,(\mu Ms)^{-1}$ and the dissociation rate of the intermediate complex is $35 \pm 2\,s^{-1}$. In a second binding step, the ligand is enclosed into the aptamer-binding pocket with a rate constant of $155 \pm 7\,s^{-1}$.

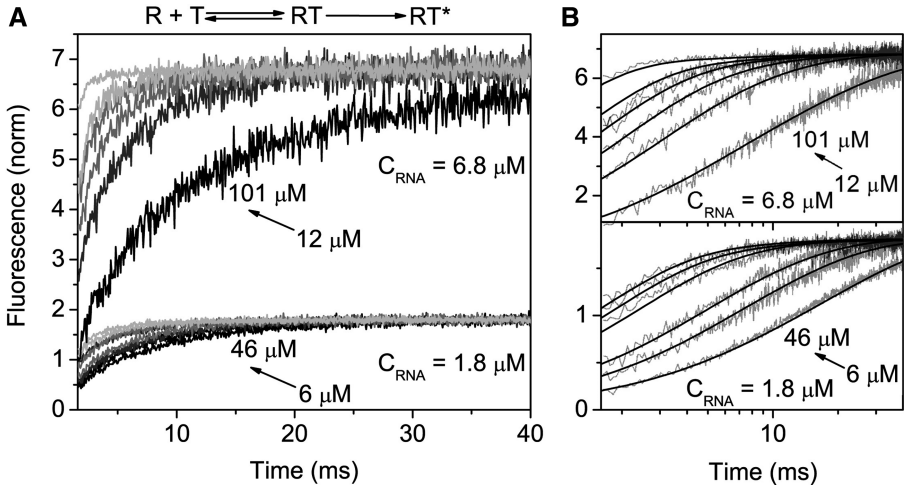

Figure 2. Binding dynamics of the wild-type aptamer in dependence of both tetracycline and RNA concentrations. The emission light was separated from the 375 nm excitation by two filters with a cut-off wavelength of 435 nm. The shown transients are an average of 40 (1.8 μM RNA) or 20 (6.8 μM RNA) individual measurements. (**A**) Selected transients for the binding process over a wide concentration range. (**B**) Data and fit using a two-step model for the binding of the ligand to the RNA.

Table 1. Tetracycline lifetime measurements and reaction constants for ligand binding to the tetracycline aptamers assuming a two-step process with an irreversible second step

	τ_1/ns	$k_1/(\mu Ms)^{-1}$	k_{-1}/s^{-1}	k_2/s^{-1}	ΔF_1/%	ΔF_2/%
WT	4.37 ± 0.04	13.1 ± 0.1	35 ± 2	155 ± 7	49.7 ± 0.2	50.3 ± 0.1
A50U	3.62 ± 0.02	7.3 ± 0.1	13 ± 2	124 ± 8	48.2 ± 0.3	51.8 ± 0.3
A13U	3.78 ± 0.02	5.50 ± 0.05	14 ± 1	78 ± 2	44.3 ± 0.3	55.7 ± 0.2
A9G	4.06 ± 0.04	60 ± 20	13000 ± 5000	51 ± 2	7 ± 1	93.1 ± 0.1

ΔF_i represent the relative contributions of step i to the total increase of fluorescence and k_i describes the corresponding rate constants.

Positions with direct contacts to the ligand have only marginal influence on the binding process

The analysis of mutants allows conclusions on the participation of different regions in the binding of the ligand. The bases A13 and A50 of the aptamer are located within the two regions J1-2 and L3, respectively, which are important for ligand binding (Figure 1C and E). Mutations at both positions (A13U and A50U) have a dramatic effect on ligand binding with a decrease in K_D by more than two orders of magnitude and render the aptamer regulatory inactive (22,24). Thereby, two direct H-bonds between the 6β-OH of tetracycline to the adenine at position 13 are missing in A13U (21). It has been assumed before, that binding to A13 occurs early in the reaction process (22). In the A50U mutant, a contact involved in correct positioning of the tetracycline counterion is removed (21). In this mutant the correct formation of loop L3 and the binding pocket will be impaired.

Two different RNA concentrations of A50U were investigated (1.8 and 7.8 μM) and the tetracycline concentration was varied from 6–52 μM and 12–190 μM, respectively. A number of transients corresponding to the different concentration ratios (see 'Materials and Methods' section) were taken and analysed. For A13U, 1.5 and 10 μM aptamer RNA was used with the tetracycline concentrations varying from 11–64 μM to 15–155 μM, respectively. Figures 3A and 4A show two different transients of A50U and A13U, respectively, in comparison with the wild-type. Inspection of the fluorescence dynamics directly shows that both mutations slow down the binding dynamics to a small but significant extent.

Analogous to the wild-type, a comparison between various reaction models was carried out on the basis of the collected data. Again, a two-step model with an irreversible second step was found as the most probable binding model (fits are shown in Figures 3B and 4B for selected transients). The fitting yielded reaction constants of $k_1 = 7.3 \pm 0.1$ $(\mu Ms)^{-1}$, $k_{-1} = 13 \pm 2\,s^{-1}$ and $k_2 = 124 \pm 8\,s^{-1}$ for A50U and $k_1 = 5.50 \pm 0.05$ $(\mu Ms)^{-1}$, $k_{-1} = 14 \pm 1\,s^{-1}$ and $k_2 = 78 \pm 2\,s^{-1}$ for A13U. Similar to wild-type, steps 1 and 2 contribute almost equally to the fluorescence intensity, with the A13U mutant showing the smallest increase in step 1 with 44.3 ± 0.3% (Table 1).

The reaction constants, especially k_2, of A50U differ only moderately from those obtained in the wild-type analysis. All three reaction constants are slowed down, leading to overall decelerated global dynamics. To analyse the relevance of the differences between the

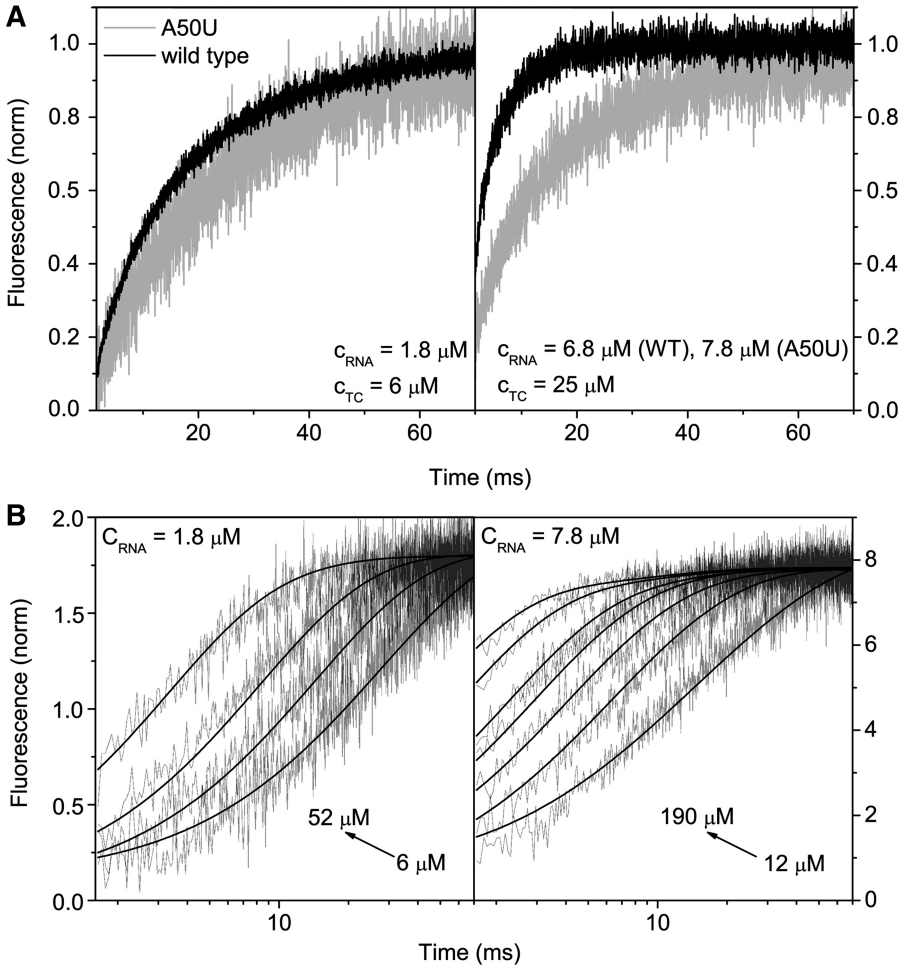

Figure 3. Binding dynamics of the A50U mutant. The emission light was separated from the 375 nm excitation by two filters with a cut-off wavelength of 435 nm. The transients shown for A50U are an average of 40 (1.8 μM RNA) or 20 (7.8 μM RNA) individual measurements. (**A**) Comparison of the wild-type and A50U dynamics at two different concentration combinations. Transients are normalized to 1 at the fluorescence maximum. (For details on the normalization procedure, see Supplementary Figure S2). (**B**) Data and fit using a two-step model for the binding of the ligand to A50U.

kinetics of A50U and wild-type, a comparison was made between different two-step models by fitting the A50U transients with a set of two-step models with either the first or the second step reaction constants fixed to those of the wild-type. A quantification of the deviation of the respective fit due to the reduction of the parameter space allows an estimate of the influences of A50 on the first and second reaction steps. Table 2 shows the fit results as well as the RMS and the Akaike value [ΔAIC; (30)], which gives an estimate on the relevance of a model compared to a reference. In this case, the reference was the above described fit of the A50U kinetics with a two-step model. The ΔAIC is dependent on both the RMS and the number of degrees of freedom in the system and thus provides an estimate on the quality of a fit.

It can be seen, that a fit with a fixed second step provides a significantly better match than the fit with a fixed first step. An Akaike value of 13 signifies a small but non-vanishing probability of ~0.2% for the model to describe the data more accurately than the reference model. An Akaike value of 880, however, signifies that there is no support for this model to describe the data. In conclusion, the base A50 exhibits a significant influence on the first binding step, and a smaller influence on the second binding step.

In contrast, the influence of A13 on both reaction steps is nearly equally strong. This is supported by the fact that a discriminative analysis between two-step models with fixed first or second steps yielded very high ΔAIC-values for both cases (5538 and 1106 for fixed first and second step, respectively). Therefore, in contrast to A50, the base A13 is highly important for both reaction steps.

Mutation of A9, involved in tertiary structure formation, yields dramatically altered binding dynamics

Mutation of A9 leads to a rise of the K_D by a factor of 210 and renders the tetracycline-binding aptamer regulatory inactive, too (22,24). The A9G mutant is lacking the central base of the base triplet formed by A44, A9 and

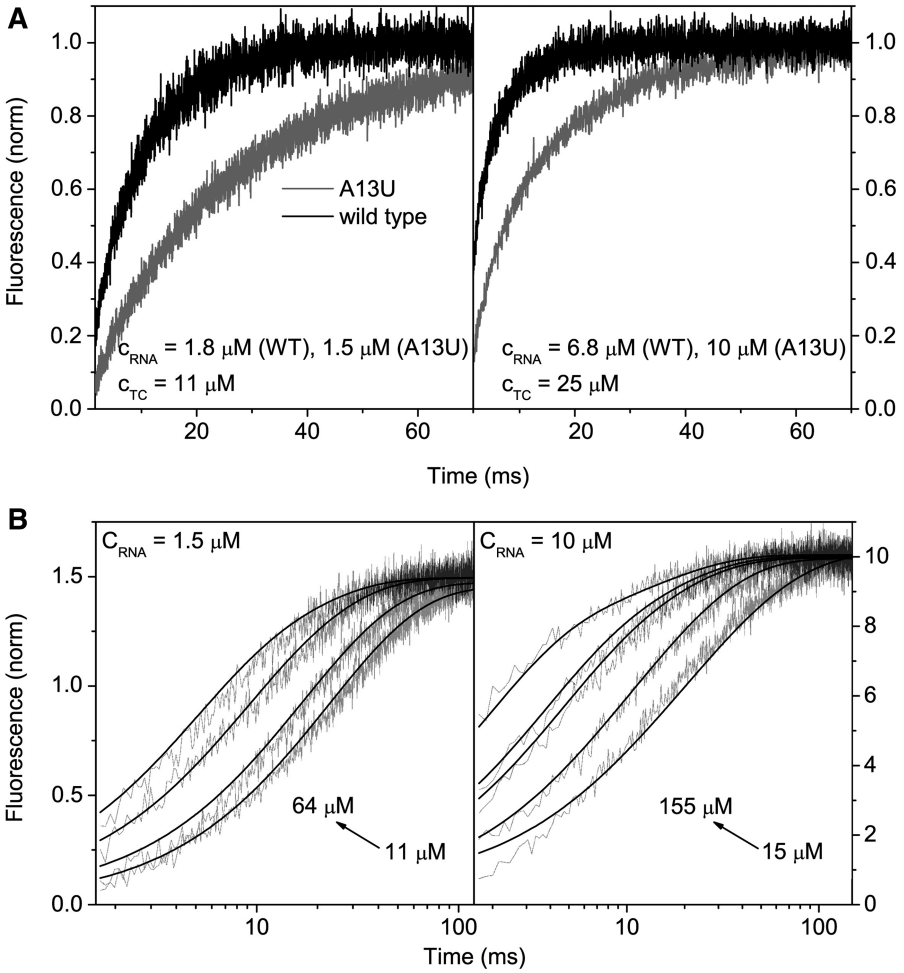

Figure 4. Binding dynamics of the A13U mutant. The emission light was separated from the 375 nm excitation by two filters with a cut-off wavelength of 435 nm. The transients shown for A13U are an average of 40 (1.5 μM RNA) or 20 (10 μM RNA) individual measurements. (**A**) Comparison of the wild-type and A13U dynamics at two different concentration combinations. Transients are normalized to 1 at the fluorescence maximum. (For details on the normalization procedure, see Supplementary Figure S2). (**B**) Data and fit using a two-step model for the binding of the ligand to A13U.

Table 2. Analysis of the differences in reaction constants between the wild-type and the mutant A50U

	$k_1/(\mu Ms)^{-1}$	k_{-1}/s^{-1}	k_2/s^{-1}	RMS	ΔAIC
WT	13.1 ± 0.1	35 ± 2	155 ± 7		–
A50U	7.3 ± 0.1	13 ± 2	124 ± 8	0.207141	0
Step 1	13.1*	35*	132 ± 2	0.221183	880
Step 2	7.59 ± 0.08	20 ± 1	155*	0.207198	13

Separate fits have been performed, where the first or second step was fixed (indicated by Asterisk) to the wild-type constants to determine the influence of the missing base A50U on the respective reaction step.

A55 which is assumed to be a key element of the tertiary structure of the tetracycline-binding aptamer (Figure 1D). Its exchange to guanine prevents the formation of three hydrogen bonds thus the three-way junction can presumably not be formed in contrast to the wild-type. It has been proposed that A9 is important for the pre-organization of the aptamer in the unbound state as the mutant is less pre-structured. This is reflected by a higher read-through in translation assays (24) and a more unfavourable binding entropy compared to the wild-type (22).

The dynamic implications of the mutation at position 9 (A9G) was examined by measurements at two different concentrations of RNA (1.8 and 9 μM) and tetracycline (6–52 and 22–228 μM), respectively. Figure 5A shows that the reaction is slowed down dramatically in comparison to the wild-type in the same concentration range.

An analysis of the reaction constants indicated that the main reason for this can be found in a drastic increase of the back reaction rate of the first reaction step ($k_{-1} = 13 \times 10^3$), which is accelerated by three orders of

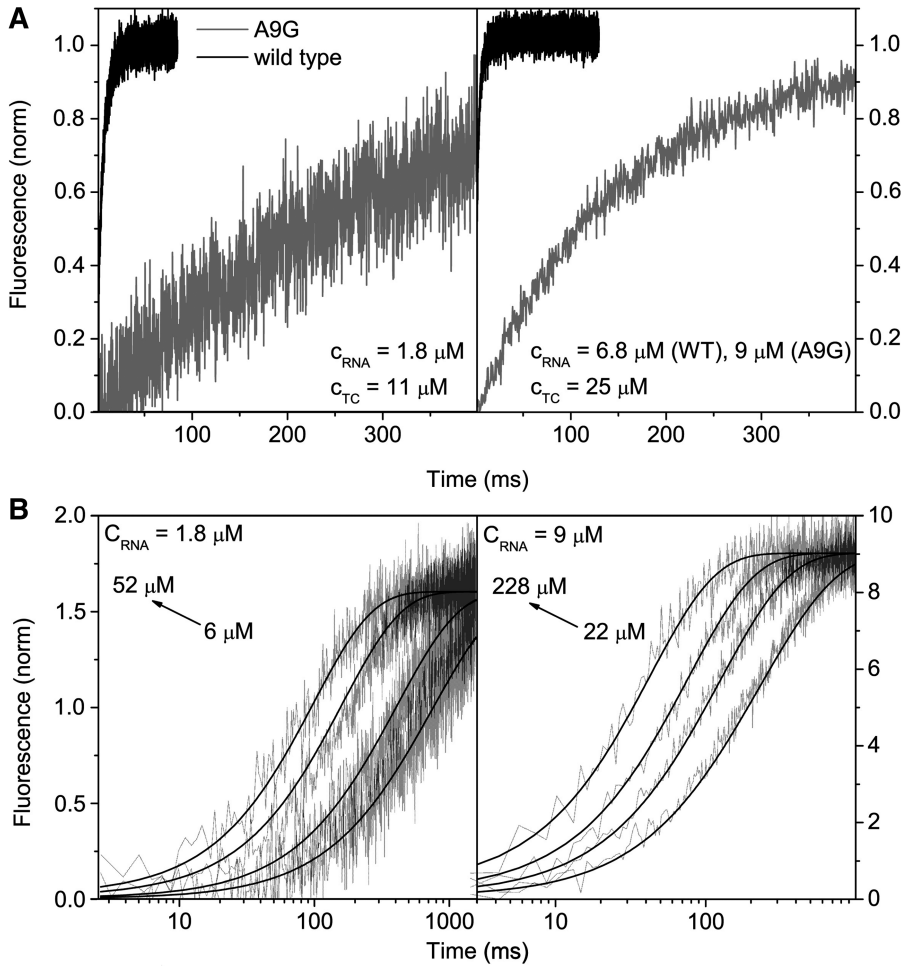

Figure 5. Binding dynamics of the A9G mutant. The emission light was separated from the 375 nm excitation by two filters with a cut-off wavelength of 435 nm. The transients shown for A9G are an average of 40 (1.8 μM RNA) or 20 (9 μM RNA) individual measurements. (**A**) Comparison of the wild-type and A9G dynamics at two different concentration combinations. Transients are normalized to 1 at the fluorescence maximum. (For details on the normalization procedure, see Supplementary Figure S2). (**B**) Data and fit using a two-step model for the binding of the ligand to A9G.

magnitude (Figure 5B and Table 1). This indicates either a masking of the correct binding site or a large number of aptamer conformations able to bind the ligand, but unable to form a correct binding pocket before the ligand dissociates again. This picture is supported by the relative fluorescence rises ΔF_1 and ΔF_2, which were also determined by the fitting routine.

It is remarkable, that the first binding step only accounts for ~7% of the total fluorescence rise, while in the wild-type and the A13U and A50G mutants it is responsible for nearly half of the total signal. The first binding step is therefore only responsible for a small conformational restriction of the ligand by the aptamer, pointing to a significantly more open conformation of this aptamer with respect to the previously examined mutants.

Tetracycline is highly restricted in the binding pocket

The excited state lifetime of a chromophore is connected to its quantum efficiency (31,32). Both are often associated with the degree of mobility that the chromophore exhibits, provided that the surroundings of the chromophore are similar in terms of other fluorescence quenching paths. The fluorescence lifetime of chromophores can be influenced by a number of environmental factors, such as solvent polarity or stacking of the chromophore with neighbouring aromatic systems.

The fluorescence of tetracycline is dependent on the vibrational de-excitation pathways allowed by its conformation and surroundings. As an example, already the complex formation of the chromophore with a counterion leads to a significantly longer excited state lifetime (33). Therefore, lifetime measurements using the Time Correlated Single Photon Counting (TCSPC) technique have been carried out on the tetracycline aptamer complex to obtain information about the binding pocket of the wild-type aptamer and the aptamer mutants A9G, A13U and A50U. Assuming that the confinement of the chromophore is the major influence of the aptamer on the tetracycline fluorescence, a comparable rise of the tetracycline fluorescence for the wild-type and the mutants would be indicative for a proper formation of a tetracycline restricting binding pocket. The crystal structure of the aptamer (21)

does not point to strong stacking interactions within the binding pocket, which could quench the fluorescence significantly. Thus, lifetime measurements of the tetracycline fluorescence reflect mainly the confinement and positioning of the chromophore in the bound state.

TCSPC measurements for the wild-type aptamer and all three mutants were performed and transients for all tetracycline aptamer complexes were collected at 470 nm (Figure 6 and Table 1). In accordance to prior studies, a non-monoexponential photophysical behaviour of the tetracycline chromophore was observed (33,34). In the cited studies, complex excited state relaxation processes such as charge transfer processes occur on the picosecond timescale which are below the time resolution of our setup. Our experiment thus only determines the overall lifetime of the lowest excited state, which can be described by a mono exponential decay for all aptamers. They show small but nevertheless significant differences due to the very accurate lifetime determination (see error for τ_1 in Table 1). Much more evident, however, is the difference in lifetime between tetracycline in buffer or with a non-specific tRNA control and the analysed tetracycline aptamer complexes (Figure 6). This indicates that—apart from subtle variations—the binding pockets of the various tetracycline aptamer complexes are properly formed.

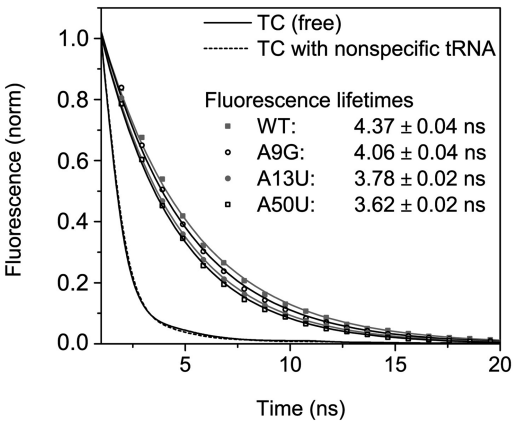

Figure 6. TCSPC measurements of the fluorescence lifetime of tetracycline (TC) alone, with non-specific tRNA or bound to the wild-type and the three mutants A9G, A13U and A50U. Excitation energy at 385 nm was tuned to 100 nJ, the transients at 470 nm are shown. Each transient is an average of 60 000 single sweeps.

The tetracycline aptamer complex with the longest lifetime of tetracycline of 4.37 ± 0.04 ns is formed with the wild-type and demonstrates the tight confinement of the chromophore within the RNA. Tetracycline bound to the A9G mutant shows a lifetime of 4.06 ± 0.04 ns whereas 3.78 ± 0.02 and 3.62 ± 0.02 ns were recorded for A13U and A50U, respectively. No photobleaching and no influence of the buffer or of non-specific RNA on the lifetime of tetracycline were observed.

The differences in fluorescence lifetime of tetracycline bound to the wild-type aptamer and the mutants are significant, but rather small. This confirms the notion derived from the steady-state fluorescence measurements, that tetracycline adapts a fixed position in the binding pocket in all aptamers. The small differences in the fluorescence lifetimes between wild-type and the mutants can be attributed to differences in the binding pockets of the analysed aptamers.

DISCUSSION

While there have been many aptamers selected for a wide variety of ligands, mostly with excellent binding properties, only very few of them can be exploited for the control of gene expression (35). This issue is the subject of ongoing discussions. A complete picture of regulating aptamers has to be obtained to understand the structural and mechanistic requirements for an aptamer functioning as engineered riboswitch. In addition to genetic, biochemical and structural studies, the conformational dynamics of aptamers has to be taken into account to shed light on the binding process. Therefore, in this study the binding kinetics of the tetracycline binding aptamer have been examined for the wild-type and three mutants (A9G, A13U, A50U) which allow conclusions on the binding mechanism involved.

The tetracycline aptamer shows a very fast binding with a two-step behaviour of the binding process. A schematic model of the binding process is depicted in Figure 7. The first binding step is reversible, while the second one does not show any significant back reaction rate. The two steps can be interpreted as a first association of the ligand with a subsequent structural reorganization of the RNA to accommodate the ligand within the binding pocket. Such a two-step-process has often been observed upon ligand binding to proteins and is usually interpreted as a

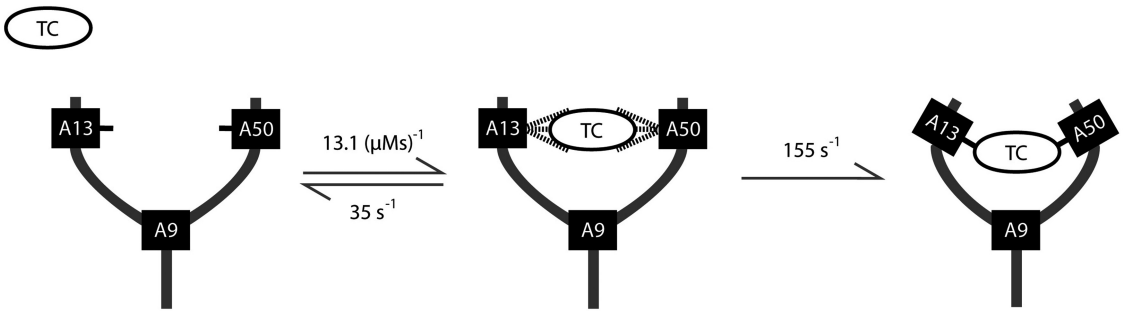

Figure 7. Schematics of the binding process of tetracycline (TC) to the aptamer as concluded from the stopped-flow measurements.

binding step with a subsequent conformational change (36,37).

The presence of significant secondary structural elements even in the absence of tetracycline would support this mechanism. Indeed structural probing indicated that large parts of the aptamer are already formed without tetracycline (24). Analytical size exclusion chromatography as well as native PAGE experiments detected no major conformational changes upon tetracycline binding (22). A preformation of the aptamer is further supported by an inhibition of gene expression already in the absence of tetracycline (17–19). EPR measurements also strongly suggest a pre-organization. Distinct label distributions indicate a ligand independent structure formation (23). The fact, that the speed of the reaction is significantly higher than for previously reported aptamer dynamics also supports the suggestion that only small structural changes occur upon ligand binding.

The two-step mechanism is in contrast to the previously observed single-step mechanisms reported for the aptamer domains of several riboswitches (8,9) and points to a distinct feature of the tetracycline aptamer. Presumably, in RNAs with more open conformations (such as the adenine riboswitch), a possible first step may not be linked to a significant fluorescence change of the ligand chromophore and may therefore not be observed in similar studies.

The single-stranded regions of the tetracycline-binding pocket form two halves opposing each other (Figure 1; J1-2 versus L3). Mutations on both sides (J1-2: A13U and L3: A50U) show an influence on the first binding step, indicating that both aptamer halves are important for the first association step. This is also reflected by the fact that the first binding step in these mutants corresponds to half of the rise in fluorescence change, like in the wild-type. The double mutant has a low K_D of $\sim$10 μM (22). It is mimicked by the measurement of A50U with doxycycline since doxycycline lacks the R6β-OH group and thus the same RNA/ligand contact as the A13U/tetracycline sample. When both contacts are missing, no increase in fluorescence is detectable (Supplementary Figure S5).

The disturbance of the second binding step in A13U is significant as well. The reaction rate is roughly half as large as in the wild-type. The reason for this can be either found in a less favourable intermediate position in A13U or in an active role of A13 during the second reaction step of the wild-type binding kinetics.

In general we only detect small influences in the association rate in the A13U and A50U mutants. We have to note that in our experiments we operate well above the K_D of all mutants (at least 10-fold on RNA and 30-fold on tetracycline level) due to a limited signal to noise ratio of the free tetracycline. It was shown before that mutants exhibiting a strong influence under equilibrium conditions can display nearly wild-type dynamics when measured under non-equilibrium conditions (38). That may also be responsible for the observation that 100% complex formation occurs, with no detectable back reaction of the second binding step.

Taken together, the absence of one of the direct contacts between the ligand and the aptamer leads to a destabilization of the binding pocket and to a moderate change in the speed of one or both binding steps. The influence on the first binding step is clearly recognizable, in both the A13U and A50U mutants.

The most striking influence on the binding process is exerted by replacement of the base A9. In the mutant A9G, the overall binding process is slowed by several orders of magnitude. The main reason for this can be found in the huge back reaction rate of the first binding step, which exceeds that of the wild-type by more than two orders of magnitude. This fact points to the idea, that there may be different conformations in A9G, which are more or less able to bind the ligand only temporarily without proceeding to the formation of a correct binding pocket before the ligand dissociates again. It is remarkable, that the first binding step only accounts for $\sim$7% of the total fluorescence rise in A9G in contrast to $\sim$50% for wild-type, A13U and A50G. This indicates that in A9G the first binding step is responsible for only a small conformational restriction of tetracycline pointing to a significantly more open conformation of the A9G mutant. In this open conformation tetracycline may be able to interact only with one of the aptamer halves during the first binding step. In the second step tetracycline forms contacts to the other half leading to the formation of the binding pocket detectable by the rise in fluorescence. Due to the more open conformation of the unbound state it is, however, very unlikely that the ligand meets an aptamer conformation that allows the formation of a correct binding pocket already during the first binding step; so that a large number of the temporarily formed complexes dissociate before correct complete formation can take place.

The reorganization of the RNA from the intermediate to the final bound state is slowed by a factor of three with respect to the wild-type. Considering, that tetracycline meets a more open conformation, this is only a small effect. The reason for the high speed of this process can be found in the fact, that only few conformations are capable of completing this step. These conformations presumably are very similar to that of the wild-type. Similar effects have already been observed and discussed for other aptamers (8,12). If such a suitable conformation is available, the formation of the ligand RNA complex occurs with a relatively high rate.

The fluorescence lifetimes indicate that the final state of the binding process and the restriction of tetracycline within the binding pocket are pretty similar for all analysed aptamers. The lifetime measurements of the bound state showed only small variations ($\tau_{WT} > \tau_{A9G} > \tau_{A13U} > \tau_{A50U}$). A9G shows the longest lifetime of the mutants which allows the conclusion that the shape of the final binding pocket itself is similar to wild-type and mostly dependent on tetracycline and its direct contacts to the RNA and less on the pre-organization of the aptamer (22).

If a direct contact between the ligand and the aptamer is missing, the chromophore is slightly more flexible within its binding pocket, as can be seen by the shorter fluorescence lifetime of tetracycline in the A13U and A50U

mutants. A50U exhibits the shortest lifetime of all examined complexes. Mutation of A50 leads to a more favourable entropy of binding, because tetracycline does not interact with loop L3 in a similar way to the wild-type, suggesting a minor loss of degrees of freedom (22).

Previous studies by EPR spectroscopy revealed a thermodynamic equilibrium of two aptamer conformations in the free form, with one of the conformations stabilized upon tetracycline binding (23). Both free conformations differ in the location of the junction J1-2 relative to stems P1 and P2 and loop L3. We suggest that displacement of junction J1-2 allows a first association of tetracycline already contacting J1-2 through A13 and/or L3 by the A50 base. A second reorganization step then leads to complete complex formation with J1-2 positioned like in the crystal structure.

The measured association rates, as well as previous findings, suggest a high degree of pre-formation of the tetracycline aptamer in the absence of its ligand, allowing for an outstanding fast association. This extraordinary fast association may be the explanation for the regulating activity of the tetracycline aptamer. Fast association is important for natural riboswitches acting on the level of transcription. These riboswitches are comprised of an aptamer domain and an expression platform, namely a transcriptional terminator. Here, ligand binding to the nascent transcript has to occur within a short time frame to stabilize the anti-terminator conformation before the terminator is transcribed (11).

In the case of the tetracycline aptamer we do not have an additional expression platform since regulation occurs via steric hindrance of the ribosomal scanning process. Still it faces a similar problem. There might be only a small time window in which the pre-formed aptamer is susceptible for ligand binding before the mRNA is covered with the translational machinery. Later on, small ribosomal subunits scanning the 5′-UTR may prevent pre-formation of the aptamer structures which are necessary for tetracycline binding. On the other side, the complex has to be rigid enough to withstand oncoming scanning ribosomes, probably reflected by the high restriction of the tetracycline in the binding pocket. Mutations interfering with one of these two features will therefore render the aptamer inactive.

SUPPLEMENTARY DATA

Supplementary Data are available at NAR Online: Supplementary Table S1 and Supplementary Figures S1–S5.

ACKNOWLDGEMENTS

The authors thank Dr Georg Wille and Prof. Dr Jens Wöhnert for helpful advice and discussions.

FUNDING

Aventis foundation (Suess group); the Deutsche Forschungsgemeinschaft via the Collaborative Research Center 902 'Molecular Principles of RNA-based Regulation' and the Cluster of Excellence 'Macromolecular Complexes' (both groups). Funding for open access charge: Collaborative Research Center 902 'Molecular Principles of RNA-based Regulation'.

Conflict of interest statement. None declared.

REFERENCES

1. Al-Hashimi,H.M. and Walter,N.G. (2008) RNA dynamics: it is about time. *Curr. Opin. Struct. Biol.*, **18**, 321–329.
2. Latham,M.P., Zimmermann,G.R. and Pardi,A. (2009) NMR chemical exchange as a probe for ligand-binding kinetics in a theophylline-binding RNA aptamer. *J. Am. Chem. Soc.*, **131**, 5052–5053.
3. Buck,J., Fürtig,B., Noeske,J., Wöhnert,J. and Schwalbe,H. (2007) Time-resolved NMR methods resolving ligand-induced RNA folding at atomic resolution. *Proc. Natl Acad. Sci. USA*, **104**, 15699–15704.
4. Noeske,J., Schwalbe,H. and Wöhnert,J. (2007) Metal-ion binding and metal-ion induced folding of the adenine-sensing riboswitch aptamer domain. *Nucleic Acids Res.*, **35**, 5262–5273.
5. Noeske,J., Buck,J., Fürtig,B., Nasiri,H.R., Schwalbe,H. and Wöhnert,J. (2007) Interplay of 'induced fit' and preorganization in the ligand induced folding of the aptamer domain of the guanine binding riboswitch. *Nucleic Acids Res.*, **35**, 572–583.
6. Wickiser,J.K., Winkler,W.C., Breaker,R.R. and Crothers,D.M. (2005) The speed of RNA transcription and metabolite binding kinetics operate an FMN riboswitch. *Mol. Cell.*, **18**, 49–60.
7. Lemay,J.F., Penedo,J.C., Tremblay,R., Lilley,D.M.J. and Lafontaine,D.A. (2006) Folding of the adenine riboswitch. *Chem. Biol.*, **13**, 857–868.
8. Gilbert,S.D., Stoddard,C.D., Wise,S.J. and Batey,R.T. (2006) Thermodynamic and kinetic characterization of ligand binding to the purine riboswitch aptamer domain. *J. Mol. Biol.*, **359**, 754–768.
9. Wickiser,J.K., Cheah,M.T., Breaker,R.R. and Crothers,D.M. (2005) The kinetics of ligand binding by an adenine-sensing riboswitch. *Biochemistry*, **44**, 13404–13414.
10. Lee,S.W., Zhao,L., Pardi,A. and Xia,T. (2010) Ultrafast dynamics show that the theophylline and 3-methylxanthine aptamers employ a conformational capture mechanism for binding their ligands. *Biochemistry*, **49**, 2943–2951.
11. Lang,K., Rieder,R. and Micura,R. (2007) Ligand-induced folding of the thiM TPP riboswitch investigated by a structure-based fluorescence spectroscopic approach. *Nucleic Acids Res.*, **35**, 5370–5378.
12. Jucker,F.M., Phillips,R.M., McCallum,S.A. and Pardi,A. (2003) Role of a heterogeneous free state in the formation of a specific RNA-theophylline complex. *Biochemistry*, **42**, 2560–2567.
13. Rieder,U., Kreutz,C. and Micura,R. (2010) Folding of a transcriptionally acting preQ1 riboswitch. *Proc. Natl Acad. Sci. USA*, **107**, 10804–10809.
14. Duchardt-Ferner,E., Weigand,J.E., Ohlenschläger,O., Schmidtke,S.R., Suess,B. and Wöhnert,J. (2010) Highly modular structure and ligand binding by conformational capture in a minimalistic riboswitch. *Angew. Chem. Int. Ed. Engl.*, **49**, 6216–6219.
15. Leulliot,N. and Varani,G. (2001) Current topics in RNA-protein recognition: control of specificity and biological function through induced fit and conformational capture. *Biochemistry*, **40**, 7947–7956.
16. Berens,C., Thain,A. and Schroeder,R. (2001) A tetracycline-binding RNA aptamer. *Bioorg. Med. Chem.*, **9**, 2549–2556.
17. Kötter,P., Weigand,J.E., Meyer,B., Entian,K.D. and Suess,B. (2009) A fast and efficient translational control system for conditional expression of yeast genes. *Nucleic Acids Res.*, **37**, e120.
18. Hanson,S., Berthelot,K., Fink,B., McCarthy,J.E.G. and Suess,B. (2003) Tetracycline-aptamer-mediated translational regulation in yeast. *Mol. Microbiol.*, **49**, 1627–1637.

19. Suess,B., Hanson,S., Berens,C., Fink,B., Schroeder,R. and Hillen,W. (2003) Conditional gene expression by controlling translation with tetracycline-binding aptamers. *Nucleic Acids Res.*, **31**, 1853–1858.
20. Weigand,J.E. and Suess,B. (2007) Tetracycline aptamer-controlled regulation of pre-mRNA splicing in yeast. *Nucleic Acids Res.*, **35**, 4179–4185.
21. Xiao,H., Edwards,T.E. and Ferré-D'Amaré,A.R. (2008) Structural basis for specific, high-affinity tetracycline binding by an in vitro evolved aptamer and artificial riboswitch. *Chem. Biol.*, **15**, 1125–1137.
22. Müller,M., Weigand,J.E., Weichenrieder,O. and Suess,B. (2006) Thermodynamic characterization of an engineered tetracycline-binding riboswitch. *Nucleic Acids Res.*, **34**, 2607–2617.
23. Wunnicke,D., Strohbach,D., Weigand,J.E., Appel,B., Feresin,E., Suess,B., Müller,S. and Steinhoff,H.J. (2011) Ligand-induced conformational capture of a synthetic tetracycline riboswitch revealed by pulse EPR. *RNA*, **17**, 182–188.
24. Hanson,S., Bauer,G., Fink,B. and Suess,B. (2005) Molecular analysis of a synthetic tetracycline-binding riboswitch. *RNA*, **11**, 503–511.
25. Takahashi,M., Degenkolb,J. and Hillen,W. (1991) Determination of the equilibrium association constant between tet repressor and tetracycline at limiting Mg^{2+} concentrations: A generally applicable method for effector-dependent high-affinity complexes. *Anal. Biochem.*, **199**, 197–202.
26. Carlotti,B., Fuoco,D. and Elisei,F. (2010) Fast and ultrafast spectroscopic investigation of tetracycline derivatives in organic and aqueous media. *Phys. Chem. Chem. Phys.*, **12**, 15580–15591.
27. Förster,U., Gildenhoff,N., Grünewald,C., Engels,J.W. and Wachtveitl,J. (2009) Photophysics of 1-ethynylpyrene-modified RNA base adenine. *J. Lumin.*, **129**, 1454–1458.
28. Kuzmic,P. (2009) *DynaFit–a Software Package for Enzymology*. Elsevier Academic Press Inc., San Diego, USA.
29. Kuzmic,P. (1996) Program DYNAFIT for the analysis of enzyme kinetic data: application to HIV proteinase. *Anal. Biochem.*, **237**, 260–273.
30. Akaike,H. (1974) New look at statistical-model identification. *IEEE Transactions On Automatic Control*, **AC19**, 716–723.
31. Birks,J.B. (1970) *Photophysics of Aromatic Molecules*. Wiley-VCWiley-Interscience, London and New York, USA.
32. Lakowicz,J.R. (1999) *Principles of Fluorescence Spectroscopy*. 2nd edn. Springer, Berlin.
33. Schneider,S., Schmitt,M.O., Brehm,G., Reiher,M., Matousek,P. and Towrie,M. (2003) Fluorescence kinetics of aqueous solutions of tetracycline and its complexes with Mg^{2+} and Ca^{2+}. *Photochem. Photobiol. Sci.*, **2**, 1107–1117.
34. Morrison,H., Olack,G. and Xiao,C. (1991) Organic photochemistry. 93. Photochemical and photophysical studies of tetracycline. *J. Am. Chem. Soc.*, **113**, 8110–8118.
35. Weigand,J.E., Sanchez,M., Gunnesch,E.B., Zeiher,S., Schroeder,R. and Suess,B. (2008) Screening for engineered neomycin riboswitches that control translation initiation. *RNA*, **14**, 89–97.
36. Burton,R.L., Hanes,J.W. and Grant,G.A. (2008) A stopped flow transient kinetic analysis of substrate binding and catalysis in Escherichia coli d-3-phosphoglycerate dehydrogenase. *J. Biol. Chem.*, **283**, 29706–29714.
37. Olsen,K., Svensson,B. and Christensen,U. (1992) Stopped-flow fluorescence and steady-state kinetic studies of ligand-binding reactions of glucoamylase from Aspergillus niger. *Eur. J. Biochem.*, **209**, 777–784.
38. Wachtveitl,J., Farchaus,J.W., Mathis,P. and Oesterhelt,D. (1993) Tyrosine 162 of the photosynthetic reaction center L-subunit plays a critical role in the cytochrome c_2 mediated rereduction of the photooxidized bacteriochlorophyll dimer in Rhodobacter sphaeroides. 2. Quantitative kinetic analysis. *Biochemistry*, **32**, 10894–10904.